Endothelial Dysfunction in the Tubule Area Accelerates the Progression of Early Diabetic Kidney Disease

Wan ZENG[1#], Daojing YING[2#], Bohan CHEN[1], Pei WANG[1]

[#] *These authors contributed equally to this study*

[1]Blood Purification Center & Department of Nephrology, the First Affiliated Hospital of Zhengzhou University, Zhengzhou, China, [2]Department of Pediatrics, the First Affiliated Hospital of Zhengzhou University, Zhengzhou, China

Received March 2, 2024
Accepted September 3, 2024

Summary

Diabetic kidney disease (DKD) is the leading cause of end-stage renal disease. Therefore, understanding the molecular regulatory mechanisms underlying the pathogenesis of DKD is imperative. In this study, we aimed to explore the molecular mechanisms of tubule region endothelial dysfunction in early DKD. Early-stage DKD model was established in 16-week-old female db/db mice for 16 weeks. Body weight, glucose level, and urine albumin-to-creatinine ratio (UACR) were measured. Hematoxylin and eosin (H&E) and periodic acid-Schiff (PAS) staining were performed to evaluate pathological lesions. RNA sequencing data of the kidneys and integrated publicly available single-cell and spatial transcriptome datasets were used to investigate the mechanism of endothelial dysfunction. There was a significant increase in body weight ($p = 0.001$), glucose levels ($p=0.0008$), and UACR ($p=0.006$) in db/db mice compared with db/m mice. H&E and PAS staining showed that vacuolar lesions and protein casts of tubules were the major histopathological changes observed in early-stage DKD mice. The apoptotic pathway in endothelial cells was notably activated in DKD, and Thbs1 was identified as the central gene involved in this apoptotic process. Deconvolution of the cell composition in the RNA sequencing data showed a decrease in the proportion of endothelial cells in the DKD mice. Further analysis of the activity and regulatory network of transcription factors showed that Creb1 was activated in both mouse and human early-stage DKD, suggesting that Creb1 activation may be involved in early kidney injury. The endothelial cell apoptotic pathway is activated in DKD, and the proportion of endothelial cells was reduced in the DKD mice, which is significantly associated with Thbs1.

Keywords

Diabetic kidney disease • Endothelial dysfunction • RNA sequencing • Thbs1 • Creb1

Corresponding author

Pei Wang, Blood Purification Center & Department of Nephrology, the First Affiliated Hospital of Zhengzhou University, No.1 Jianshe East Road, Erqi District, Zhengzhou City, Henan Province, 450052, China. Email: wpei@zzu.edu.cn

Introduction

Diabetic kidney disease (DKD) is a major microvascular complication of diabetes mellitus (DM). Approximately 30–40 % of DM patients develop DKD [1], and nearly half of all DKD cases progress to end-stage renal disease [2]. Several factors lead to the development of DKD, including clinical risk factors, disease management, heredity, kidney structural changes, and abnormal activation or suppression of signaling pathways [3]. Increasing evidence indicates that endothelial cell dysfunction is crucial in the glomerular pathogenesis of DKD [4]. However, the detailed molecular mechanisms of endothelial cell dysfunction in tubule area of DKD are poorly understood.

The traditional “glomerulocentric” paradigm for DKD pathology includes mesangial expansion, capillary surface reduction, and podocyte loss [5]. However, some patients with advanced DKD do not exhibit several glomerular pathologies or experience proteinuria [6]. Recently, proximal tubulopathy has been identified as a key therapeutic target for DKD [7]. Tubulointerstitial lesions are thought to be more pivotal than glomerular damage in DKD progression, and tubular epithelial cells can regulate spatially connected glomerular endothelial cells [8]. Thus, we focus on the role of tubulopathy in DKD pathogenesis. The mouse model has been extensively used

to study human diseases. Currently, two mutant mouse models, db/db and BTBR ob/ob mutant models have been established to explore human DKD, which has pathological impairments similar to those of human DKD [9, 10]. The db/db mutant mouse model mimics the early-stage DKD progression [9], whereas the BTBR ob/ob mutant mouse model imitates the features of final-stage DKD [10]. Studies involving both models are important for understanding the entire progression and pathogenesis of human DKD.

High-throughput sequencing has dramatically accelerated research on disease progression. Although bulk RNA sequencing can elucidate gene expression profiles, it cannot dissect the origin of biological alterations in specific cells. Single-cell RNA sequencing (scRNA-seq) can resolve tissue heterogeneity but not the spatial information of individual cells [11]. Spatial transcriptomic analysis can provide an intuitive landscape of tissue structure in situ [12]. Therefore, an integrated multi-omics approach is necessary to comprehensively elucidate molecular changes that occur during disease progression. Therefore, we aimed to elucidate the molecular mechanisms underlying endothelial cell dysfunction in early-stage DKD using mutant diabetic mice (db/db) and multi-omics analyses, which could benefit the diagnosis and treatment of DKD.

Materials and Methods

Mouse model of DKD

All animal procedures were conducted according to protocols approved by the Institutional Animal Care and Use Committee of Zhengzhou University (ZZU-LAC202305269 [18]). The study complied with the ARRIVE guidelines. To establish an early-stage DKD mouse model, we used female mice to reduce the risk of hyperglycemic induced pyelonephritis [13, 14], and the 6 weeks db/db and db/m mice (BKS-Lepr^{em2Cd479}/Gpt, T002407) were purchased from GemPharmatech (Nanjing, China). All mice were housed to 16 weeks at 20–24 °C under a 12 h dark/light cycle, with ad libitum access to food and water. Body weight was measured at 6 weeks as well as 16 weeks, and only mice had similar body weight were used for the experiment. The serum, urine, and kidney samples of model mice were collected at 16 weeks.

Biochemical index detection

Mice in each group were fasted for 12 hours, and tail vein blood was taken. Fasting blood glucose level was measured by Accu-Chek Active blood glucose meter (Shanghai Yiyao Scientific Instrument Co., Ltd., Shanghai, China). The mice were sacrificed and urine was collected. The sediment was removed by low-speed low-temperature centrifuge, and the supernatant was taken for albumin content determination. Urine albumin and serum creatinine were measured using an automatic biochemical analyzer with a commercially available albumin-to-creatinine detection kit (Nanjing Jiancheng Bioengineering Institute, Nanjing, China). Urine albumin-to-creatinine ratio (UACR) was calculated.

Hematoxylin and eosin (H&E) staining

H&E staining was performed with an H&E staining kit (ThermoFisher, MA, USA) following the manufacturer's protocol. Part of the mouse kidney tissue was fixed with 4 % paraformaldehyde, dehydrated, and embedded in paraffin. Paraffin-embedded sections (thickness 5 μm) were baked, dewaxed with xylene, dehydrated with gradient ethanol, stained with hematoxylin for 5 min, and stained with eosin for 2 min. Pathological changes were observed under an optical microscope (OLYMPUS BX41, OLYMPUS, Tokyo, Japan).

Periodic acid-Schiff (PAS) staining

PAS staining was performed with a PAS staining kit (Shanghai Lianmai Bioengineering Co., Ltd., Shanghai, China) under the manufacturer's protocol. The kidney tissue was fixed with 4 % paraformaldehyde, dehydrated and embedded, and 5 μm thick paraffin sections were prepared. Paraffin sections were dewaxed with xylene, dehydrated with gradient ethanol, and rinsed with running water. The PAS staining was performed for 5 min and rinsed with running water. Hydrochloric acid ethanol differentiation, water washing. Gradient ethanol dehydration, xylene transparent, and neutral gum seals. Pathological changes were observed under an optical microscope (OLYMPUS BX41, OLYMPUS, Tokyo, Japan).

Bulk RNA sequencing and data processing

To construct the cDNA library for RNA sequencing, we used the NEBNext Ultra RNA Library Prep Kit for Illumina (E7530L, New England Biolabs, Ipswich, MA, USA) according to the manufacturer’s instructions. Briefly, we extracted total RNA from the whole kidney tissues and enriched mRNA from total RNA

using oligo(dT)-conjugated magnetic beads after quality control. The fragmented mRNA was used to synthesize the cDNA. PCR amplification procedures were used for library construction. The cDNA library was sequenced using a 150 bp paired-end protocol on an Illumina NovaSeq 6000 (Illumina, San Diego, CA, USA). Bioinformatic analysis of sequencing data was performed using R (version 4.2.1). The sequences were mapped to the mm10 genome using hisat2 [15], the mRNA read counts were quantified using feature counts [16], and the gene transfer format file used in gene annotation was "gencode.vM23.annotation.gtf". Differentially expressed genes (DEGs) were identified using the DESeq2 package, and principal component analysis (PCA) was performed using ggord [17]. The correlation of each sample was calculated using Spearman's test and visualized using a heatmap. Statistical significance was set at $p \leq 0.05$. Additional bulk RNA sequencing data of db/db kidney cortex and control groups were downloaded from GSE222778.

Human bulk RNA sequencing

The bulk RNA sequencing dataset for human early-stage DKD was downloaded from GSE142025. Raw RNA sequencing data were mapped to the genome using hisat2 [15], and RNA read counts were quantified using featureCounts [16]. The alignment reference genome was hg38, and the gene transfer format file for gene annotation was "gencode.v36.annotation.gtf" (downloaded from GENCODE; https://www.gencodegenes.org/).

Gene set enrichment analysis (GSEA)

Gene ontology (GO) and Kyoto Encyclopedia of Genes and Genomes (KEGG) GSEA were performed using clusterProfiler [18]. The input genes were ordered by fold changes that were calculated using DESeq2. All DEGs between the DKD versus the control groups were included. The gene SYMBOL was converted to ENTREZID using the "bitr" function, and "gseGO" and "gseKEGG" functions of clusterProfiler were used for enrichment. The normalized enrichment scores (NES) and p-values of the GSEA results were visualized using a bar plot, and the enrichment networks were visualized using aPEAR. The enriched GO terms for the transforming growth factor (TGF)-β signaling pathway were analyzed using Metascape (metascape.org/gp/index.html, v3.5.20230501) [19]. Protein–protein interaction (PPI) analysis was performed using STRING (https://cn.string-db.org/, v12.0).

Immune cell deconvolution

To characterize the immune and stromal cell compositions in early-stage DKD and control kidneys, we deconvoluted the cell proportions in the RNA sequencing data using mMCPcounter [20]. The RNA sequencing input gene expression matrix was normalized to transcripts per million. The genome version used was GCRm38. The estimated immune and stromal proportions were visualized using stacked bar plots. Differences in the immune proportion between the two groups were calculated using the Kruskal–Wallis test. The correlation of the estimated cell proportion was calculated using Pearson's test.

Transcription factor (TF) activity prediction

The activity of TFs in mouse and human DKD kidneys was predicted based on the gene expression of regulons using NetAct [21]. The regulatory interactions between TFs were identified according to their activity. The TF gene regulatory network topology was filtered by link relations based on mutual information and entropy. The constructed gene regulatory network was simulated using RACIPE (v1.16.0) to validate and evaluate the gene expression dynamics in the core network [22].

2.10. scRNA-seq

To explore the expression score of Creb1-targeted upregulated regulons, we downloaded the scRNA-seq data from GSE184652. This dataset contained db/db mice housed for 18 weeks, followed by injection with ReninAAV (2 days and 2 weeks) to mimic progressive human DKD. The db/db mice were uninephretomized and the db/m mice were treated with sham surgery. The treatments included Grp1 (db/m 2 days), Grp2 (db/db 2 days), Grp3a (db/db ReninAAV 2 days), and Grp3b (db/db ReninAAV 2 weeks). We integrated the scRNA-seq dataset using harmony (v0.1.1) [23]. The expression module score of Creb1-targeted upregulated regulons was calculated using the "AddModuleScore" function in Seurat (v4.3.0) [24], and the control features were set to 100. We visualized the expression score in each cell using a violin plot, and comparisons between the DKD and control groups were performed using the Wilcoxon test. Statistical significance was set at $p < 0.05$.

Spatial transcriptome analysis

We downloaded the ob/ob spatial RNA sequencing dataset from GSE190094 to explore the spatial expression patterns of the target genes. For Slide-seqV2 spatial transcriptome sequencing dataset analysis, we

imputed the gene expression matrix of each cell using the "RunALRA" function in SeuratWrappers (v0.3.1) to recover the real gene expression. The gene ensembles in the Slide-seqV2 dataset were converted into symbols for visualization of gene expression.

Statistical analysis

SPSS 26.0 (International Business Machines, corp., Armonk, NY, USA) was used for all statistical analysis. Data are expressed as means ± standard deviation (SD). Differences between groups were examined for statistical significance by t-test. Two-sided p-values were calculated, and $p < 0.05$ was considered to be statistically significant.

Results

Tubule pathology of early-stage DKD in db/db mice

To explore the pathogenesis of early-stage DKD, we performed bulk RNA sequencing and histopathological analysis of the kidney tissues of 16-week-old db/db and db/m mice. Multi-omics analysis integrated the bulk RNA sequencing data of early-stage human DKD (GSE142025), scRNA-seq data of db/db and db/m mice (GSE184652), and spatial RNA sequencing data of ob/ob mice (GSE190094) (Fig. 1a). Physiological and biochemical analyses showed a significant increase in body weight (p=0.001), glucose levels (p=0.0008), and UACR (p=0.006) in db/db mice compared with db/m mice (Fig. 1b–1d).

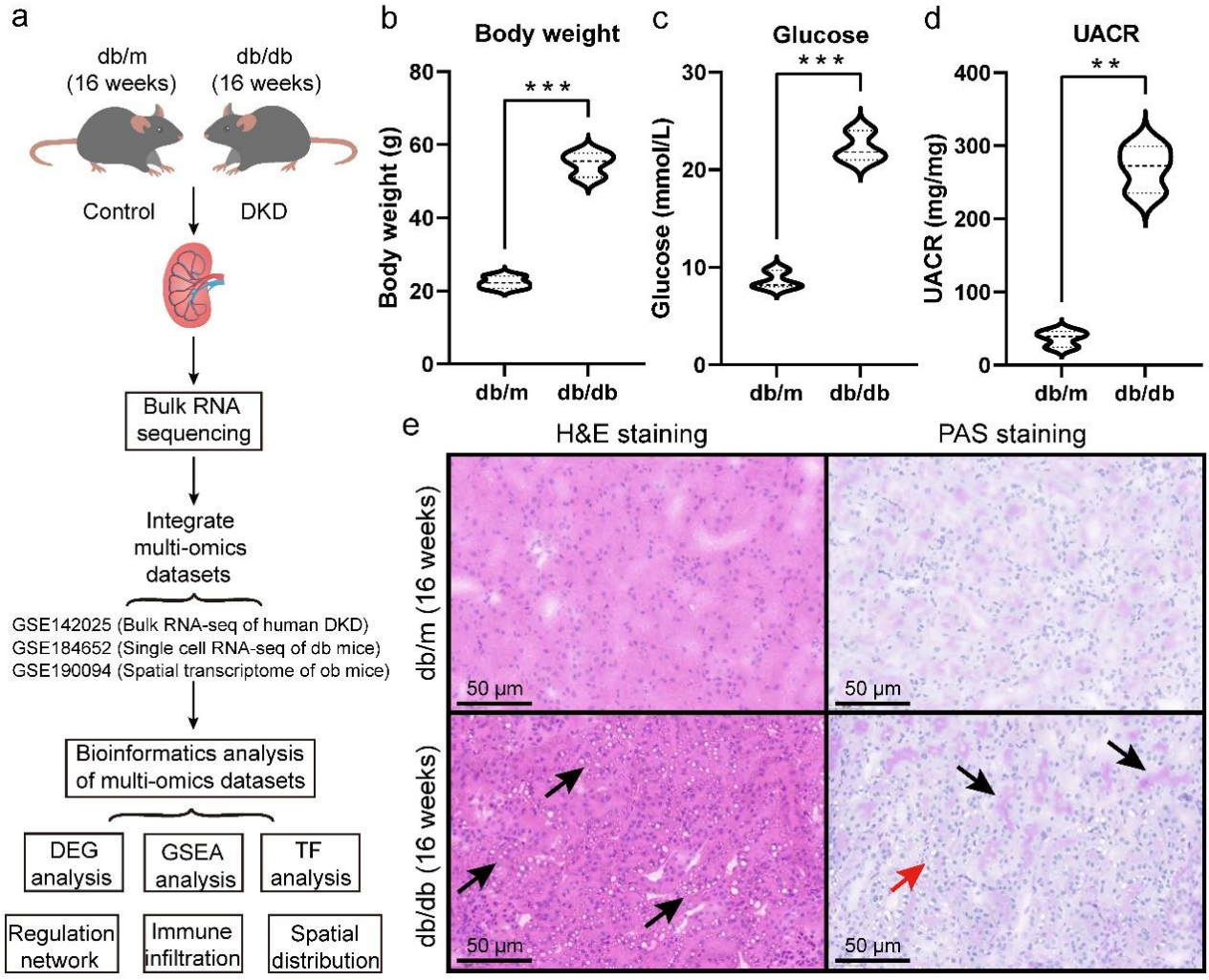

Fig. 1. Overview of study design for investigating early diabetic kidney disease (DKD). (**a**) The schematic of the research workflow; (**b**) Body weight; (**c**) glucose level; and (**d**) urine albumin-to-creatinine ratio (UACR) of 16-week-old db/m control and db/db DKD mice; (**e**) Hematoxylin and eosin (H&E; left panel) and periodic acid-Schiff (PAS; right panel) staining of the kidney of 16-week-old db/m (top panel) and db/db (bottom panel) mice. ***p<0.001; **p<0.01.

H&E and PAS staining showed that vacuolar lesions and protein casts of tubules were the major histopathological changes in early-stage DKD mice (Fig. 1e). Collectively, these results indicate the early-stage DKD mouse model is successfully established, and that the tubular injury is the major pathological lesion during early-stage DKD.

Thbs1 is involved in endothelial cell dysfunction in early-stage DKD

To elucidate the mechanism of endothelial cell dysfunction, we performed RNA sequencing of kidney samples from 16-week-old db/db and db/m mice. PCA showed that the samples in the two groups were well separated (Fig. 2a) and formed two distinct clusters

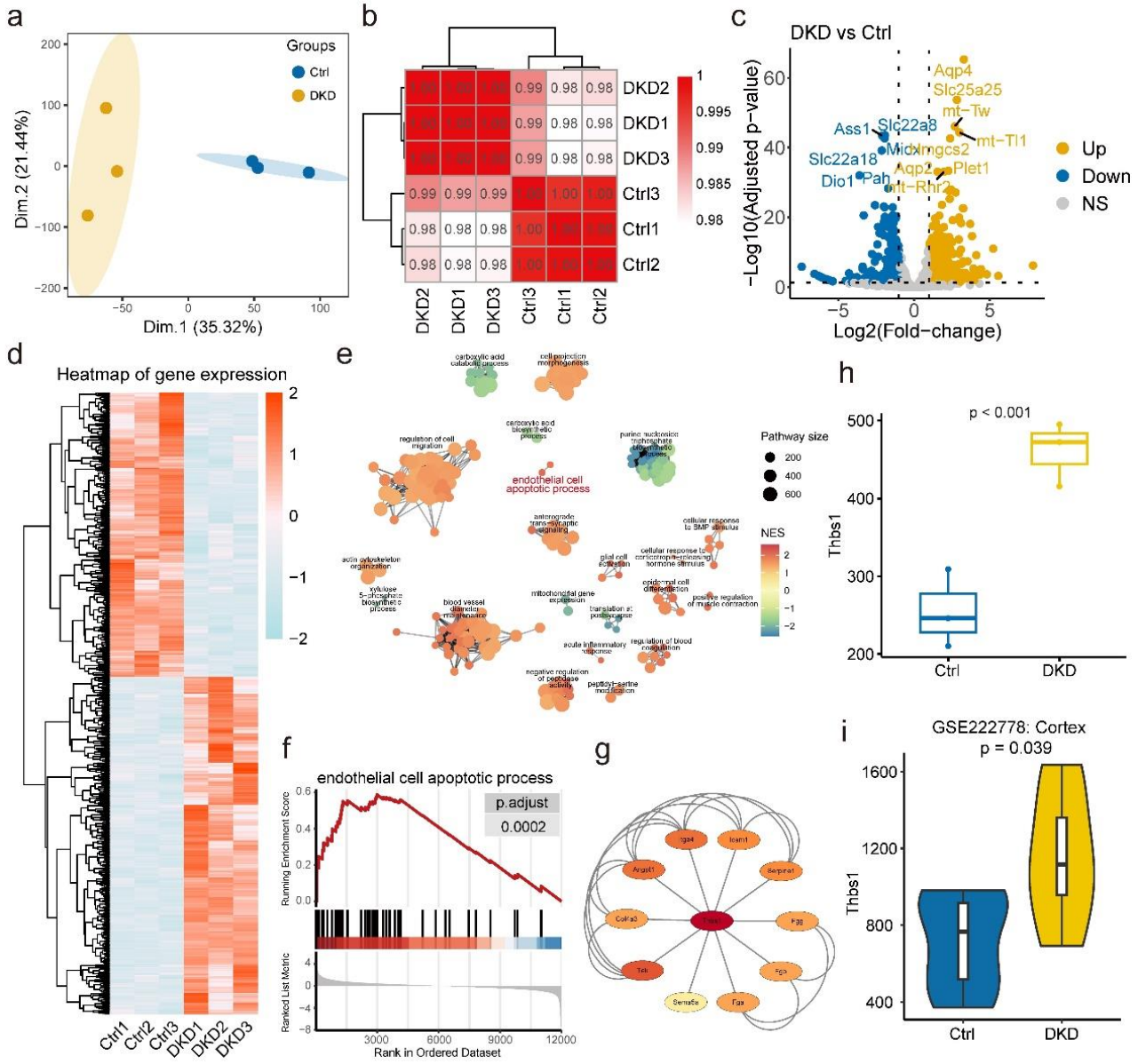

Fig. 2. Bulk RNA sequencing of db/db DKD mouse. (**a**) Principal component analysis (PCA) of RNA sequencing data of the DKD and control (Ctrl) mice (n=3); (**b**) Sample correlation analysis of bulk RNA sequencing data; (**c**) Volcano plot of differentially expressed genes (DEGs) between the DKD mice versus control mice; (**d**) Heatmap of significant DEGs; (**e**) Gene ontology (GO) enrichment network of gene set enrichment analysis (GSEA) results; (**f**) Visualization of the endothelial cell apoptosis pathway in GSEA. The x-axis is the fold-change ordered genes and the y-axis is the enrichment score of the endothelial cell apoptosis pathway. (**g**) Protein–protein interaction (PPI) analysis of endothelial cell apoptosis pathway genes using the STRING database; (**h**) Box plot of Thbs1 expression in whole kidney samples from the DKD and control groups; (**i**) Violin plot of Thbs1 expression in the kidney cortex of DKD and control groups in the GSE222778 dataset.

(Fig. 2b), suggesting considerable alterations in the transcriptome profile of the mice during disease progression. In total, 687 upregulated and 781 downregulated DEGs were identified (adjusted $p < 0.05$) and visualized using a volcano plot (Fig. 2c) and heatmap (Fig. 2d). GO enrichment network GSEA (Fig. 2e) showed that endothelial cell apoptosis was significantly activated in early-stage DKD mice compared with healthy controls (Fig. 2f). PPI analysis showed that Thbs1 was the central hub gene in the network (Fig. 2g). Thbs1 was significantly upregulated (adjusted $p < 0.001$) in db/db mice compared with db/m mice (Fig. 2h). Compared with the control group, Thbs1 was significantly upregulated in the renal cortex of mice with early-stage DKD in the GSE222778 dataset (Fig. 2i). Collectively, these results suggest that Thbs1 contributes to endothelial cell dysfunction in early-stage DKD through the apoptotic pathway.

Spatial distribution of Thbs1 in BTBR ob/ob DKD mice

To explore the potential function of Thbs1 in endothelial cell dysfunction in early-stage DKD, we analyzed the spatial gene expression pattern of Thbs1 in the kidneys of 13-week-old BTBR ob/ob mice, which mimic early-stage human DKD [25]. Specifically, we visualized spatial cell types, including endothelial cells, mesangial cells, podocytes, and epithelial cells in the thick ascending limb of Henle's loop (Fig. 3a). The spatial expression areas of Thbs1 and Pecam1 (specifically expressed in blood and vascular cells) were highly concordant with epithelial cells present in the thick ascending limb of Henle's loop (Fig. 3b, c). Therefore, Thbs1 upregulation in early-stage DKD mice may contribute to endothelial dysfunction in the thick ascending limb of Henle's loop area. In addition to biological process alterations, we performed KEGG enrichment analyses of DEGs between the early-stage DKD and control groups. The TGF-β signaling pathway was significantly activated (adjusted $p < 0.001$) in the early-stage DKD group (Fig. 3d), which was mainly involved in response to stimulus (Fig. 3e). Collectively, these results indicate that Thbs1 regulates endothelial cell dysfunction through the TGF-β signaling pathway in early-stage DKD.

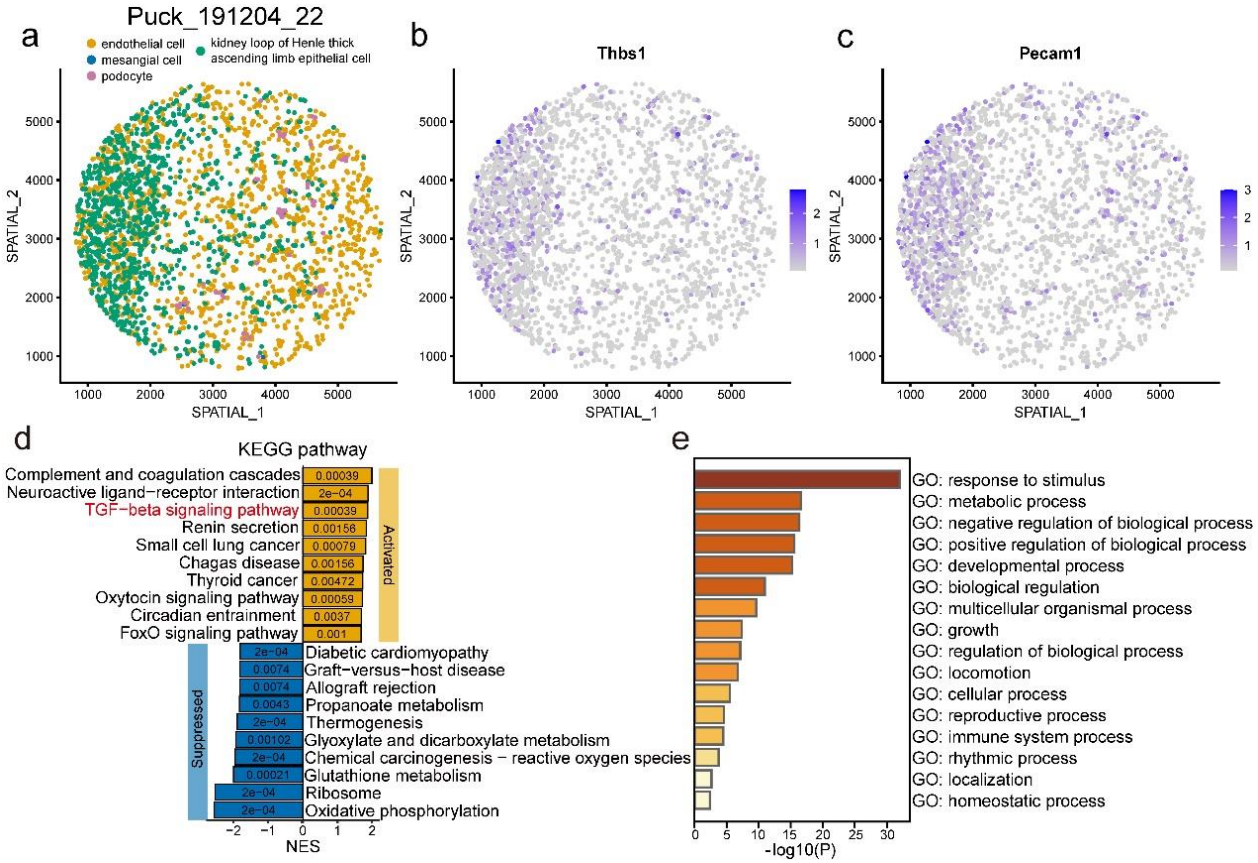

Fig. 3. The spatial expression pattern of Thbs1 in BTBR ob/ob mice. (**a**) Selected cell types mapped in spatial context of BTBR ob/ob mice kidney. (**b-c**) The spatial expression pattern of Thbs1 (**b**) and Pecam1 (**c**) in DKD. (**d**) The enriched activated and suppressed KEGG pathways in DKD mice versus control. (**e**) The enriched GO terms of TGFβ signaling pathway by Metascape.

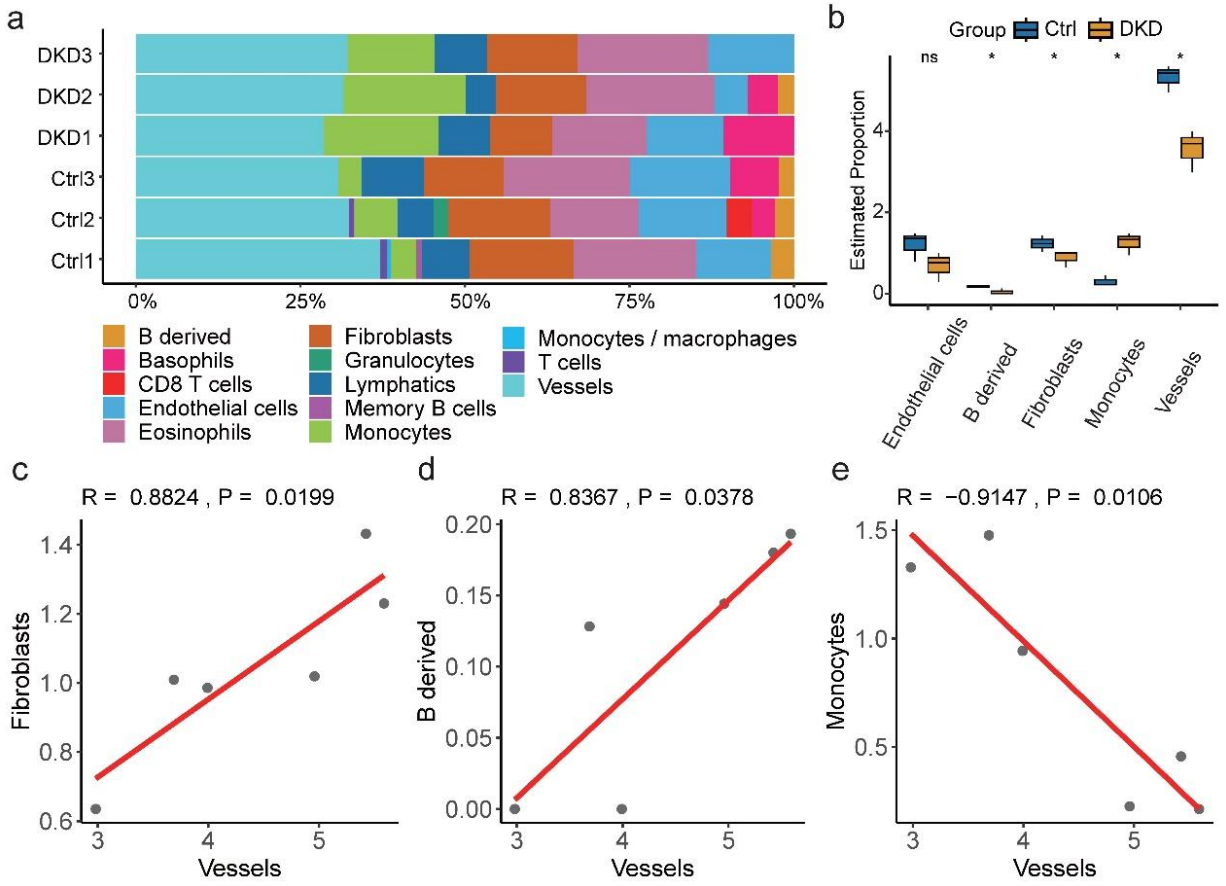

Fig. 4. The composition of cells in the kidneys of db/db and db/m mice. (**a**) Immune and stromal cell proportions were deconvoluted using mMCPcounter; (**b**) Differences in the proportions of endothelial cells, B-derived cells, fibroblasts, monocytes, and vessel cells between the DKD and control groups. (**c–e**) Correlation of fibroblasts, B-derived cells, and monocytes with vessel cells. *p<0.05; ns, p>0.05.

Relationship between immune infiltration and endothelial dysfunction

To reveal the association between immune cell infiltration and endothelial cell injury, we deconvoluted the cell composition in both normal and early-stage DKD kidneys (Fig. 4a). The proportion of endothelial cells was decreased in db/db mice compared with that in db/m mice (p=0.127, Fig. 4b), which was consistent with the observed activation of endothelial cell apoptosis in early-stage DKD (Fig. 2f). Compared with the levels in healthy kidneys, there was a significant decrease in the proportions of B-derived cells, fibroblasts, and vessel cells, and an increase in monocytes in the kidneys of db/db mice ($p < 0.05$, Fig. 4b). Endothelial cells formed the inner layer of vessels, making them crucial for maintaining function [26]. Therefore, we examined the correlations of fibroblasts, B-derived cells, and monocytes with vessel cells. All three cell types were significantly correlated with vessel cells ($p < 0.05$, Fig. 4c–4e). These results indicate that endothelial cell dysfunction is strongly associated with pathological kidney lesions in early-stage DKD and that monocytes are the major infiltrating immune cells in patients with early-stage DKD.

TF activity and regulatory network in early-stage DKD

To investigate the gene regulatory network involved in the pathogenesis of DKD, we characterized the activities of TFs in early-stage DKD. Cebpb, Creb1, Pparg, Rela, Sp1, and Rxra were significantly activated in the DKD group compared with the control group (Fig. 5a), and Creb1 was an essential gene in the TF regulatory network (Fig. 5b). To evaluate the dynamics of the core network, we simulated the model dynamic behavior of the constructed network. The PCA model plot was consistent with the diverse gene expression patterns in the DKD and control experimental data (Fig. 5c). Additionally, CREB1 was significantly activated in the kidneys of individuals with early-stage DKD in comparison with the controls ($p < 0.0001$, Fig. 5d), which was consistent with the findings in the DKD mouse model. PPI analysis of Creb1-targeted

upregulated genes showed that Jun, Fos, and Stat3 were crucial hub genes regulated by Creb1 (Fig. 5e). Additionally, Jun, Fos, and Stat3 were significantly upregulated in the early-stage DKD group compared with the healthy control group (Fig. 5f–5h).

To reveal the mechanisms of Creb1-regulated genes in DKD pathogenesis, the Creb1 regulon score of endothelial cells was determined using a publicly available scRNA-seq dataset of db/db mice. Creb1 regulon score was significantly higher in the DKD db/db mice than in the db/m control mice (Fig. 6a). The hub gene expression pattern in the spatial context of ob/ob diabetic mice (Fig. 6b) showed that the spatial expression patterns of Creb1, Jun, and Stat3 highly overlapped (Fig. 6c–6e), indicating that Creb1 regulated the expression and activity of Jun and Stat3 in an autocrine manner. Moreover, the spatial expression patterns of Creb1, Jun, and Stat3 overlapped with that of the endothelial cell marker Emcn (Fig. 6f), suggesting that Creb1 may be involved in endothelial dysfunction in early-stage DKD.

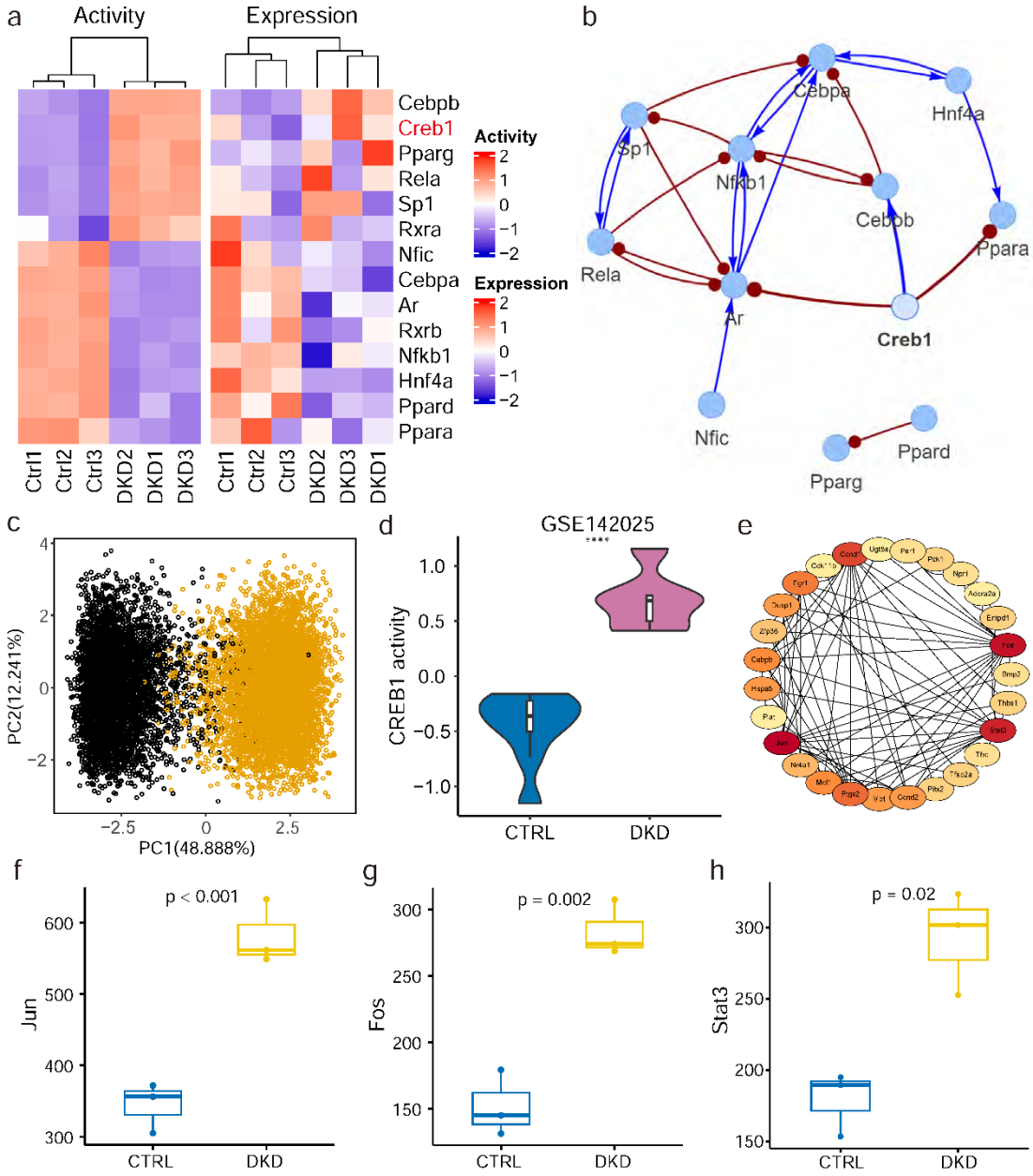

Fig. 5. Activated TFs in DKD and control mice. (**a**) The activities of TFs in the DKD and control groups were analyzed using NetAct; (**b**) The regulatory network of TFs in DKD progression; (**c**) PCA plot of simulated model dynamic behavior using RACIPE; (**d**) The predicted CREB1 activity in patients with early-stage DKD and healthy controls; (**e**) PPI analysis of Creb1-targeted genes using the STRING database; (**f–h**) The gene expression of Jun, Fos, and Stat3 in DKD and control mice. ****p<0.0001.

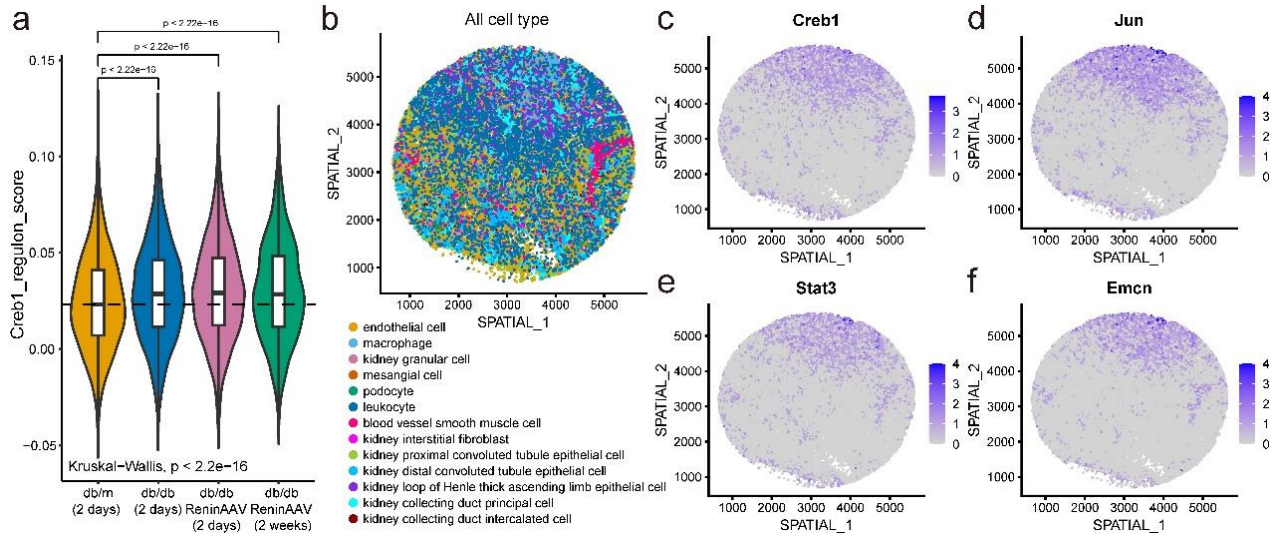

Fig. 6. Creb1 regulon expression pattern within endothelial cells in both single-cell and spatial context. (**a**) The expression score of Creb1 regulons in endothelial cells of db/db DKD mice in the GSE184652 dataset; (**b**) Cell type mapping in the spatial transcriptome data of ob/ob DKD mice from the GSE190094 dataset; The spatial expression features of (**c**) Creb1, (**d**) Jun, (**e**) Stat3, and (**f**) Emcn in ob/ob mice.

Discussion

DKD is the leading cause of end-stage renal disease, affecting patients' well-being and increasing the healthcare burden worldwide. In this study, we attempted to elucidate the underlying mechanism of endothelial cell dysfunction in DKD using a db/db mice model. The RNA sequencing data obtained in DKD db/db mice were compared to publicly available human and mouse datasets. We systematically analyzed the molecular features of the endothelial cell apoptotic pathway in DKD db/db mice using bulk RNA sequencing, scRNA-seq, and spatial expression levels. Endothelial cell apoptosis was significantly activated in early-stage DKD mice, which was consistent with a previous finding that showed that endothelial dysfunction is a potential contributor to DKD pathogenesis [27]. This result indicates that endothelial cell apoptosis may be a therapeutic target for DKD.

Thbs1 plays a central role in endothelial apoptosis through the TGF-β signaling pathway within the thick ascending limb of Henle's loop area. Generally, DM patients have a higher THBS1 expression than healthy individuals [28]. Moreover, the TGF-β canonical pathway upregulates THBS1 expression in gliomas [29]. Previous studies about DKD have mainly focused on renal glomerular malfunction. However, injury to the thick ascending limb of Henle's loop area has not been previously reported. These results provide novel insights into the pathogenesis of early-stage DKD.

Immune infiltration and inflammation are crucial for DKD pathogenesis. Therefore, we examined the proportions of both immune and stromal cells in the kidneys of db/db and healthy mice. There was a decrease in the proportions of endothelial cells and a significant decrease in B cells, fibroblasts, and vessel cells in db/db mice. In contrast, monocytes were increased in early-stage DKD mice. It has been reported that macrophages are the main contributors to DKD pathogenesis [30]. Other types of monocytes may also play important roles in DKD injury. Therefore, further exploration of monocyte heterogeneity may improve the understanding of DKD pathogenesis. Overall, there is increasing evidence to support the contribution of immune response and inflammation to the pathogenesis and progression of DKD [2]. Endothelial dysfunction may lead to pathological damage in DKD and induce immune cell infiltration, which may accelerate DKD progression.

Creb1 is activated in both mouse and human early-stage DKD, and it is involved in endothelial cell resistance to inflammation and apoptosis [31]. Therefore, Creb1 activation might be due to a stress response to immune cell infiltration and inflammation, which is consistent with the observed relationship between TGF-β pathway activation and response to stimulus. Creb1 may be involved in the regulation of endothelial cell dysfunction. Crucial hub genes regulated by Creb1 (Jun, Fos, and Stat3) were significantly upregulated in early-stage DKD. Endothelial STAT3 activation has been shown to increase vascular leakage in human diabetic retinopathy [32], and Jun upregulation induced endothelial cell barrier

dysfunction in a hemorrhage shock model [33]. Collectively, these results suggest that Creb1 induces Stat3 and Jun activation, which are detrimental to endothelial function.

A major limitation of this study is the use of a mouse model. Although the mouse model is well-established and useful for investigating human DKD, it is difficult to define DKD developmental stages in terms of time points because human diseases are complex and heterogeneous. Therefore, further studies are necessary to construct a systematic time axis for the DKD mouse model to align with the progression of human DKD.

In conclusion, the endothelial cell apoptotic pathway is activated in DKD mice, and the proportion of endothelial cells is reduced in the DKD mice. Thbs1 is identified as the central gene involved in the endothelial cell apoptotic process, particularly in cells in the thick ascending limb of Henle's loop. Creb1 is activated in both mouse and human early-stage DKD, suggesting that Creb1 activation may be involved in early kidney injury. Overall, these results provide novel insights into the regulatory networks in endothelial dysfunction in early-stage DKD, and potential targets for DKD diagnosis and therapy.

Data Availability Statement

The bulk RNA sequencing data in our study were deposited in GEO with the accession number PRJNA1009142. Human bulk RNA sequencing data of patients with early-stage DKD and normal controls were downloaded from GSE142025. Bulk RNA sequencing of db/db kidney cortex and control groups was downloaded from GSE222778. Single-cell RNA sequencing data of db/db mice were downloaded from GSE184652. Spatial transcriptome data of ob/ob mice sequenced using Slide-seqV2 were downloaded from GSE190094.

Conflict of Interest

There is no conflict of interest.

Acknowledgements

This research was funded by the National Natural Science Foundation of China (grant number 81873612).

Institutional Review Board Statement: The animal study protocol was approved by the Institutional Animal Care and Use Committee of Zhengzhou University (protocol code ZZU-LAC20230526 [18]; date of approval: May 26, 2023).

References

1. Alicic RZ, Rooney MT, Tuttle KR. Diabetic kidney disease: challenges, progress, and possibilities. Clin J Am Soc Nephrol 2017;12: 2032-2045. https://doi.org/10.2215/CJN.11491116
2. Tang SCW, Yiu WH. Innate immunity in diabetic kidney disease. Nat Rev Nephrol 2020;16:206-222. https://doi.org/10.1038/s41581-019-0234-4
3. Fu H, Liu S, Bastacky SI, Wang X, Tian XJ, Zhou D. Diabetic kidney diseases revisited: A new perspective for a new era. Mol Metab 2019;30:250-263. https://doi.org/10.1016/j.molmet.2019.10.005
4. Lassén E, Daehn IS. Molecular mechanisms in early diabetic kidney disease: glomerular endothelial cell dysfunction. Int J Mol Sci 2020;21. https://doi.org/10.3390/ijms21249456
5. Rovin BH. Beyond a glomerulocentric view of inflammation. Kidney Int 2001;60:797-798. https://doi.org/10.1046/j.1523-1755.2001.060002797.x
6. Krolewski AS. Progressive renal decline: the new paradigm of diabetic nephropathy in type 1 diabetes. Diabetes Care 2015;38:954-962. https://doi.org/10.2337/dc15-0184
7. Gilbert RE. Proximal Tubulopathy: Prime mover and key therapeutic target in diabetic kidney disease. Diabetes 2017;66:791-800. https://doi.org/10.2337/db16-0796
8. Chen SJ, Lv LL, Liu BC, Tang RN. Crosstalk between tubular epithelial cells and glomerular endothelial cells in diabetic kidney disease. Cell Prolif 2020;53: e12763. https://doi.org/10.1111/cpr.12763
9. Sharma K, McCue P, Dunn SR. Diabetic kidney disease in the db/db mouse. Am J Physiol Renal Physiol 2003;284: F1138-1144. https://doi.org/10.1152/ajprenal.00315.2002
10. Hudkins KL, Pichaiwong W, Wietecha T, Kowalewska J, Banas MC, Spencer MW, et al. BTBR Ob/Ob mutant mice model progressive diabetic nephropathy. J Am Soc Nephrol 2010;21:1533-1542. https://doi.org/10.1681/ASN.2009121290

11. Tang F, Barbacioru C, Wang Y, Nordman E, Lee C, Xu N, et al. mRNA-Seq whole-transcriptome analysis of a single cell. Nat Methods 2009;6: 377-382. https://doi.org/10.1038/nmeth.1315
12. Longo SK, Guo MG, Ji AL, Khavari PA. Integrating single-cell and spatial transcriptomics to elucidate intercellular tissue dynamics. Nat Rev Genet 2021;22: 627-644. https://doi.org/10.1038/s41576-021-00370-8
13. Luo W, Tang S, Xiao X, Luo S, Yang Z, Huang W, et al. Translation animal models of diabetic kidney disease: biochemical and histological phenotypes, advantages and limitations. Diab, Metab Synd Obesity 2023;16:1297-1321. https://doi.org/10.2147/dmso.S408170
14. Harlan SM, Heinz-Taheny KM, Sullivan JM, Wei T, Baker HE, Jaqua DL, et al. Progressive Renal Disease Established by Renin-Coding Adeno-Associated Virus–Driven Hypertension in Diverse Diabetic Models. J Am Soc Nephrol 2018;29:477-491. https://doi.org/10.1681/asn.2017040385
15. Kim D, Paggi JM, Park C, Bennett C, Salzberg SL. Graph-based genome alignment and genotyping with HISAT2 and HISAT-genotype. Nat Biotechnol 2019;37:907-915. https://doi.org/10.1038/s41587-019-0201-4
16. Liao Y, Smyth GK, Shi W. featureCounts: an efficient general purpose program for assigning sequence reads to genomic features. Bioinformatics 2014;30: 923-930. https://doi.org/10.1093/bioinformatics/btt656
17. Love MI, Huber W, Anders S. Moderated estimation of fold change and dispersion for RNA-seq data with DESeq2. Genome Biol 2014;15:550. https://doi.org/10.1186/s13059-014-0550-8
18. Yu G, Wang LG, Han Y, He QY. clusterProfiler: an R package for comparing biological themes among gene clusters. OMICS 2012;16:284-287. https://doi.org/10.1089/omi.2011.0118
19. Zhou Y, Zhou B, Pache L, Chang M, Khodabakhshi AH, Tanaseichuk O, et al. Metascape provides a biologist-oriented resource for the analysis of systems-level datasets. Nat Commun 2019;10: 1523. https://doi.org/10.1038/s41467-019-09234-6
20. Petitprez F, Levy S, Sun CM, Meylan M, Linhard C, Becht E, et al. The murine Microenvironment Cell Population counter method to estimate abundance of tissue-infiltrating immune and stromal cell populations in murine samples using gene expression. Genome Med 2020;12:86. https://doi.org/10.1186/s13073-020-00783-w
21. Su K, Katebi A, Kohar V, Clauss B, Gordin D, Qin ZS, et al. NetAct: a computational platform to construct core transcription factor regulatory networks using gene activity. Genome Biol 2022;23:270. https://doi.org/10.1186/s13059-022-02835-3
22. Huang B, Jia D, Feng J, Levine H, Onuchic JN, Lu M. RACIPE: a computational tool for modeling gene regulatory circuits using randomization. BMC Syst Biol 2018;12:74. https://doi.org/10.1186/s12918-018-0594-6
23. Korsunsky I, Millard N, Fan J, Slowikowski K, Zhang F, Wei K, et al. Fast, sensitive and accurate integration of single-cell data with Harmony. Nature Methods 2019;16: 1289-1296. https://doi.org/10.1038/s41592-019-0619-0
24. Hao Y, Hao S, Andersen-Nissen E, Mauck WM, 3rd, Zheng S, Butler A, et al. Integrated analysis of multimodal single-cell data. Cell 2021;184: 3573-3587 e3529. https://doi.org/10.1016/j.cell.2021.04.048
25. Marshall JL, Noel T, Wang QS, Chen H, Murray E, Subramanian A, et al. High-resolution Slide-seqV2 spatial transcriptomics enables discovery of disease-specific cell neighborhoods and pathways. iScience 2022;25:104097. https://doi.org/10.1016/j.isci.2022.104097
26. Trimm E, Red-Horse K. Vascular endothelial cell development and diversity. Nat Rev Cardiol 2023;20:197-210. https://doi.org/10.1038/s41569-022-00770-1
27. Nakagawa T, Tanabe K, Croker BP, Johnson RJ, Grant MB, Kosugi T, et al. Endothelial dysfunction as a potential contributor in diabetic nephropathy. Nat Rev Nephrol 2011;7: 36-44. https://doi.org/10.1038/nrneph.2010.152
28. Tang X, Miao Y, Luo Y, Sriram K, Qi Z, Lin FM, et al. Suppression of endothelial AGO1 promotes adipose tissue browning and improves metabolic dysfunction. Circulation 2020;142:365-379. https://doi.org/10.1161/CIRCULATIONAHA.119.041231
29. Daubon T, Leon C, Clarke K, Andrique L, Salabert L, Darbo E, et al. Deciphering the complex role of thrombospondin-1 in glioblastoma development. Nat Commun 2019;10: 1146. https://doi.org/10.1038/s41467-019-08480-y
30. Fu J, Sun Z, Wang X, Zhang T, Yuan W, Salem F, et al. The single-cell landscape of kidney immune cells reveals transcriptional heterogeneity in early diabetic kidney disease. Kidney Int 2022;102:1291-1304. https://doi.org/10.1016/j.kint.2022.08.026

31. Mylroie H, Dumont O, Bauer A, Thornton CC, Mackey J, Calay D, et al. PKCepsilon-CREB-Nrf2 signalling induces HO-1 in the vascular endothelium and enhances resistance to inflammation and apoptosis. Cardiovasc Res 2015;106:509-519. https://doi.org/10.1093/cvr/cvv131
32. Yun JH, Park SW, Kim KJ, Bae JS, Lee EH, Paek SH, et al. Endothelial STAT3 Activation Increases Vascular Leakage Through Downregulating Tight Junction Proteins: Implications for Diabetic Retinopathy. J Cell Physiol 2017;232:1123-1134. https://doi.org/10.1002/jcp.25575
33. Wu F, Wang JY, Dorman B, Zeineddin A, Kozar RA. c-Jun-mediated miR-19b expression induces endothelial barrier dysfunction in an in vitro model of hemorrhagic shock. Mol Med 2022;28:123. https://doi.org/10.1186/s10020-022-00550-0